METHODS: A Companion to Methods in Enzymology 18, 231–239 (1999)
Article ID meth.1999.0776, available online at http://www.idealibrary.com on IDEAL®

Two-Photon Imaging in Living Brain Slices

Z. F. Mainen, M. Maletic-Savatic, S. H. Shi, Y. Hayashi, R. Malinow, and K. Svoboda[1]

Cold Spring Harbor Laboratory, 1 Bungtown Road, Cold Spring Harbor, New York 11724

Two-photon excitation laser scanning microscopy (TPLSM) has become the tool of choice for high-resolution fluorescence imaging in intact neural tissues. Compared with other optical techniques, TPLSM allows high-resolution imaging and efficient detection of fluorescence signal with minimal photobleaching and phototoxicity. The advantages of TPLSM are especially pronounced in highly scattering environments such as the brain slice. Here we describe our approaches to imaging various aspects of synaptic function in living brain slices. To combine several imaging modes together with patch-clamp electrophysiological recordings we found it advantageous to custom-build an upright microscope. Our design goals were primarily experimental convenience and efficient collection of fluorescence. We describe our TPLSM imaging system and its performance in detail. We present dynamic measurements of neuronal morphology of neurons expressing green fluorescent protein (GFP) and GFP fusion proteins as well as functional imaging of calcium dynamics in individual dendritic spines. Although our microscope is a custom instrument, its key advantages can be easily implemented as a modification of commercial laser scanning microscopes.

To gain an understanding of the dynamics of neuronal circuits, neurons have to be studied in preparations that are as intact as possible. For many questions of subcellular physiology, the living brain slice offers an attractive compromise between the obvious limitations of cultured neurons and the experimental difficulties encountered when working with intact animals. One problem with brain slice physiology has been that scattering makes traditional optical microscopies difficult in living tissues (1). However, over the last 10 years, the development of new optical techniques with an ability to penetrate scattering tissues has contributed to a revolution in quantitative cellular physiology in brain slices. Infrared differential interference contrast microscopy (IRDIC) allows the visualization of neuronal somata and dendrites up to ~80 μm deep in brain slices, facilitating high quality whole cell patch clamp recordings under visual control (2, 3). Two-photon excitation laser scanning microscopy (TPLSM) (4) allows high resolution fluorescence imaging in brain slices up to several hundred micrometers deep with minimal phototoxicity and photobleaching (1, 5–8). In our laboratory we use IRDIC, TPLSM, and a laser-based DIC technique, implemented on a custom-built microscope, to study synaptic function in neocortical and hippocampal brain slices. In this article we describe our instrument and discuss its performance. To appreciate our design decisions, a brief review of imaging in scattering tissues is given. For more complete discussions see Ref. (1, 9).

Brain slices are hostile to traditional microscopies. In conventional wide-field fluorescence microscopy, scattering degrades resolution and contrast. In confocal microscopy, resolution and contrast are recovered by placing an aperture in front of the detector. The aperture will reject off-focus light, but it will also reject signal that has been scattered on its way out of the tissue. This is a severe drawback because a vast majority of signal photons can be scattered. Compensating for the signal loss by increasing the illumination intensity leads to increased photodamage. The result is that for a given signal level more excitation events have to occur, producing increased phototoxicity and photobleaching. For many applications requiring high resolution imaging in slices, the compromise between efficient signal detection and high-resolution is not practical and that is where TPLSM comes in.

In TPLSM, two long-wavelength (IR) excitation photons combine to excite a visible fluorophore. This results in a nonlinear relationship between excitation

[1] To whom correspondence should be addressed. Fax: (516) 367–6805. E-mail: svoboda@cshl.org.

1046-2023/99 $30.00

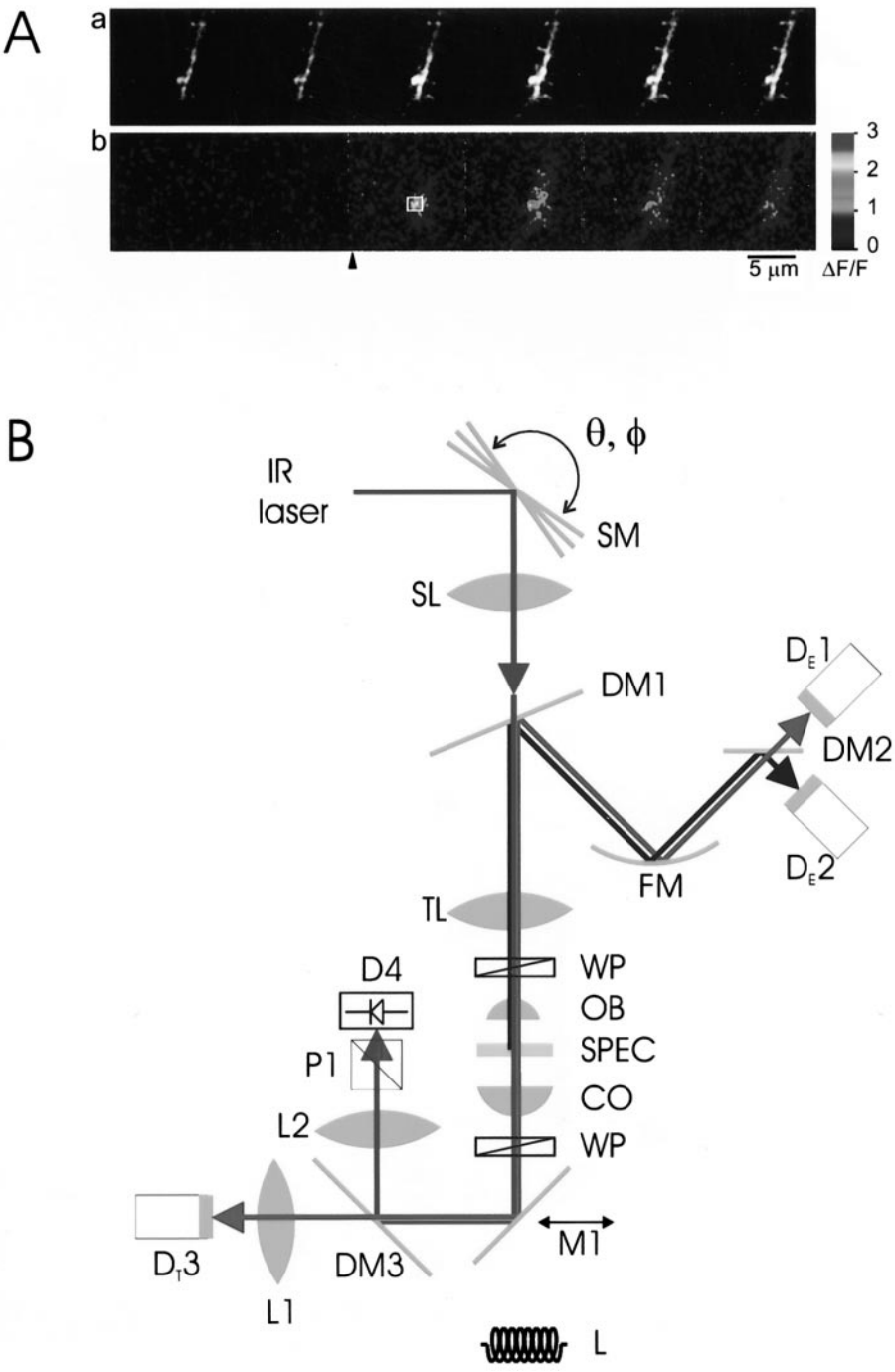

FIG. 1. (A) Measurement of synaptic transmission at individual dendritic spines using the movie mode. Single trial is measured using a time series of fluorescence images (128 × 128 pixels) acquired at 256 ms/frame. At the beginning of the third frame, transmission was evoked with an electrical shock (arrow). The Ca^{2+} indicator was OGB-1 (400 μM). (a) Raw fluorescence image. (b) Normalized change in fluorescence. (B) Optical train of our brain slice microscope. The entire microscope is translated on an X–Y table, while the laser is fixed on the optical bench (not shown). Using routing mirrors (not shown) the IR laser excitation beam is directed to a pair of scan mirrors (SM). The scan mirrors are imaged into the backfocal plane of the objective (OB) using the scan lens (SL) and tube lens (TL). The beam also passes through a Wollaston prism (WP). In our setup the WP serves to implement wide-field IRDIC microscopy and is also involved in laser scanning DIC (LSDIC). The objective focuses the laser to a diffraction-limited spot in the specimen plane (SPEC), where the fluorescence signal is generated. The IR laser light is used further for LSDIC. The light is collected by the condenser (CO). The condenser backfocal plane is imaged through a second Wollaston prism and a polarizer (P1) onto a photodiode detector (D4) using a lens (L2). The dichroic mirror (DM3) directs the IR light to the photodiode and also helps to reduce background due to IR light on the PMT (D_T3). Fluorescence is detected in either epifluorescence (D_E1, D_E2) or transfluorescence (D_T3) mode (of course, both wavelengths could be detected in trans- and epifluorescence modes). In epifluorescence the signal is reflected by a dichroic mirror (oriented at 22.5° to minimize aberrations in the laser beam) and focused

rates and incident light flux with several useful consequences. First and foremost, excitation is localized to the tiny focal volume ($<1\ \mu m^3$), which by itself is sufficient to produce three-dimensional, diffraction-limited resolution and sectioning. Scattered excitation light bounces around, too dilute to excite. In addition, compared with one-photon microscopic techniques, the longer wavelength of the excitation light is scattered less and leads to better penetration into the tissue. Because of the localization of fluorescence, a pinhole is not necessary to reject off-focus radiation, and both scattered and ballistic fluorescence photons can be collected as useful signals. The excellent photodamage properties of TPLSM allow functional imaging of calcium concentration ($[Ca^{2+}]$) at individual dendritic spines (Fig. 1) over hundreds of trials. Tissue penetration depths up to 500 μm have been demonstrated, even in the intact brain (10, 11).

INSTRUMENTATION

Although commercial instruments are becoming available (Bio-Rad), custom design allowed us to optimize our microscope for slice imaging at relatively low cost. The key issues for imaging in slices will be explicitly described; all of these can be implemented rather easily by modifying commercial confocal laser scanning microscopes. The basic light train is shown in Fig. 1 (see figure legend for details).

General Setup

The microscope is based on a vertical rail (Newport, X-95) mounted on a sturdy X–Y stage (NEAT, XYR 80-80). The optical components can easily be adjusted up- and downward along the rail. The specimen and electrophysiological manipulators are rigidly attached to the optical bench for maximal stability. This arrangement can offer excellent access for electrode placement Focusing is achieved by moving the objective. Our IRDIC setup does not differ substantially from published versions (2) and will therefore not be described in detail.

Excitation Light

A TPLSM microscope is essentially a simplified laser scanning confocal microscope, where the light source is a mode-locked pulsed laser (12). Lasers producing subpicosecond pulses at ~100 MHz are the only light sources that provide sufficient excitation for TPLSM. For slice imaging, 5- to 100-mW laser power has to be delivered to the specimen; of course, due to scattering only a small fraction remains to form the focus. This requires lasers producing >200-mW average powers. We used a commercial Ti:sapphire laser (Mira 900F, Coherent) pumped by an 8-W argon ion laser (Innova 310, Coherent). Using a single filter set (Mid-Wave), this laser can be conveniently tuned from $\lambda = 780$ nm to 910 nm. This is a useful feature since different fluorophores might require different excitation wavelengths. For example, to image either dynamics using Calcium Green 1 and Oregon-BAPTA Green 1 (Molecular Probes, Eugene, OR) we tune the laser to $\lambda \sim 800$ nm; to image EGFP, $\lambda \sim 900$–910 nm (13) works best. The laser delivers ~100-fs pulses at the rate of 76 MHz. In our experiments, one-photon damage due to the excitation laser or lack of two-photon excitation power was never limiting. We therefore did not use dispersion compensation (14, 15). Before entering the microscope, the beam diameter was increased to 2–3 mm with a mirror-based telescope. A pair of coupling mirrors were used to transfer the beam from the reference frame of the optical bench onto the X–Y stage carrying the microscope and into a pair of scanning mirrors (Cambridge Instruments, 6800). Each of the coupling mirrors moves with one direction of the stage; the result is that the beam remains aligned in the reference frame of the stage when the stage is moved. The scan mirrors were imaged into the backfocal plane of the objective (60×, 0.9 NA) by a scan lens and the microscope tube lens (both from Zeiss). Using appropriate components (mirrors and lenses optimized for near IR), more than 70% of the laser power can be delivered into the back of the objective. When converting a commercial scanner for TPLSM, dichroic mirrors and some types of dielectric mirrors have to be replaced. One can also be surprised by very strong absorption in objectives and scan and tube lenses that are not optimized for IR transmission, especially at $\lambda >$ 850 nm. Microscope manufacturers nowadays reluctantly release transmission and reflection curves for most optical components. Some companies (notably Olympus and Zeiss) produce lines of optics optimized for the near-IR wavelength regime.

onto a pair of detectors using a focusing mirror (FM). The coating of this dielectric mirror (BD1, Newport) efficiently reflects the visible signal while transmiting infrared radiation, helping to reduce background due to the IR laser light. A dichroic mirror (DM2) is used to send two emission wavelengths (blue and green) to detectors (D_E1 and D_E2, respectively). In transfluorescence the signal is passed through a dichroic mirror (DM3) and focused onto a PMT (D_T3). PMTs D_E1, D_E2, and D_T3 are all protected from IR stray light using appropriate blocking filters. For green light, color glass filters offer cheap alternatives to dielectric mirrors with excellent transmission in the visible (~98%) but not in the IR ($\sim 10^{-4}$). For red fluorescence we use custom bandbass filters (Chroma Technologies). A sliding mirror (M1) serves to switch between wide-field IRDIC using a tungsten light source (L) and laser scanning modes. Reproduced here in black and white. See special color plate section for reproduction in color.

Beam Scanning and Data Collection

In terms of beam scanning and data collection, TPLSM does not differ much from confocal microscopy [see, e.g., Ref. (16) for a collection of reviews]. A notable exception involves scanning by acousto-optic deflector, as implemented in some fast confocal microscopes (Noran). Unfortunately these fast devices are not readily well suited for TPLSM because severe dispersion will destroy the pulse train.

Detection

Since two-photon excitation produces true localization of excitation, all fluorescence constitutes useful signal and a pinhole is not necessary to reject off-focus signal. This implies that in TPLSM the photodetector does not need to be located in a conjugate image plane. Fluorescence is typically detected through the objective (epifluorescence). As has been pointed out before (9), it is actually advantageous to directly image the backfocal plane onto the detector (whole-field detection). In this way, all of the light collected by the objective can be directed to the detector and the image on the detector does not move. Whole-field detection is probably the most important modification when converting a confocal microscope for TPLSM.

A more ambitious but equally advantageous improvement can be achieved by collecting additional fluorescence signal through the condenser (transfluorescence). This falls into the category of "external detection" (9). Since the collection efficiency is proportional to $\sim NA^2$, approximately twice as much signal can be collected through our condenser (NA = 1.4, Zeiss) as through the objective (typical NAs for water immersion objectives are <1.0). For optimal signal-to-noise ratio improvements the gains for both channels have to be matched. However, for the same photomultiplier (PMT) voltage one cannot assume the same PMT gain (i.e., charge per photon). We have seen variations as large as 40% in our small sample of tubes (Hamamatsu R3896). We do the tweaking at the level of the preamplifier; alternatively, two separately controlled high-voltage power supplies can be used. The signals from the PMTs can be combined using a simple summing amplifier (17).

An evaluation of epifluorescence and transfluorescence detection is shown in Fig. 2. Dendritic structures labeled with EGFP were imaged with transfluorescence and epifluorescence detection (E+T) or epifluorescence (E) or transfluorescence (T) detection alone. The T signal was larger than the E signal by a factor of $\sim$2.8. Part of this difference ($\sim$25%) is due to differing detector quantum efficiencies in our setup. For the E signal we used an off-the-shelf PMT, while the T signal was detected using a custom-selected PMT. The remainder of the difference, a factor of $\sim$2, is due to the larger NA of our oil immersion condenser compared with our objective. To assess the effects of scattering on signal detection, we compared the collection efficiencies of the E and T pathways at the upper surface of the slice and deep in the slice ($\sim$200 μm) (data not shown). If scattering were to reduce our collection efficiency, the ratio should decrease as a function of depth in the slice. In other words, the T pathway should perform relatively better deep in the slice, while the E pathway should perform better close to the surface. Our experiments revealed that E signal/T signal is essentially constant, independent of imaging depth up to 200 μm below the surface of the slice. Thus, scattering does not seem to reduce collection efficiencies.

New Detector Technologies

PMTs have significant shortcomings as photodetectors. Their quantum efficiency is limited ($<$30% at peak for "selected tubes"; significantly less above 600 nm). In addition they generate considerable multiplicative noise due to pulse height variability. This multiplicative noise is equivalent to a signal loss of 30–40% compared with a noiseless detector. But a clear

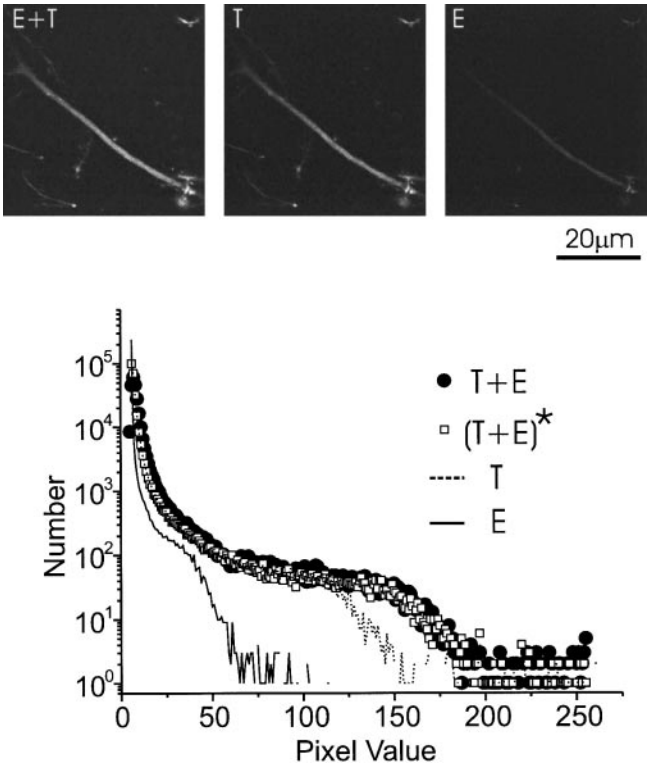

FIG. 2. Comparison of signal levels with epifluorescence (E) and transfluorescence (T) detection. (Top) Dendritic structures labeled with EGFP imaged with epi- and transfluorescence detection (E+T); transfluorescence detection (T); and epifluorescence detection (E). (Bottom) Distributions of pixel values for the three detection modes. In addition, the plot also shows the distribution of pixel values for the sum of images acquired with epi- and transfluorescence alone, (T+E)*.

alternative detector technology has not emerged. Avalanche photodiodes (EGG Canada) have much improved quantum efficiencies (>50%), but they have to be used in photon counting mode at low count rates (<5 MHz), not sufficiently fast for many applications. In addition, their sensitive areas are small (<0.5 mm), creating a difficult optical problem in cramming all fluorescence photons onto the detector. The so-called Intensified Photodiode (Intevac) also produces improved quantum efficiencies and reduced multiplicative noise. But its gain is small (1000 electrons/photon) and it produces spurious large events at appreciable rates. In addition its cost is high.

Laser Scanning DIC

Since the polarized light of the infrared laser is passed through the Wollaston prisms used by the IRDIC, only one additional polarizer and photodetector are necessary to implement laser scanning DIC (LSDIC) (Fig. 1). This imaging mode has drawbacks compared with wide-field IRDIC; for example, the relatively slow refresh rate makes it inconvenient for visually guided whole-cell recordings. But some features of LSDIC make it complementary to IRDIC. In particular, The LSDIC image is automatically aligned to submicrometer precision with the fluorescence image; it therefore allows precise placement of a stimulating electrode with respect to fluorescent structures (see below).

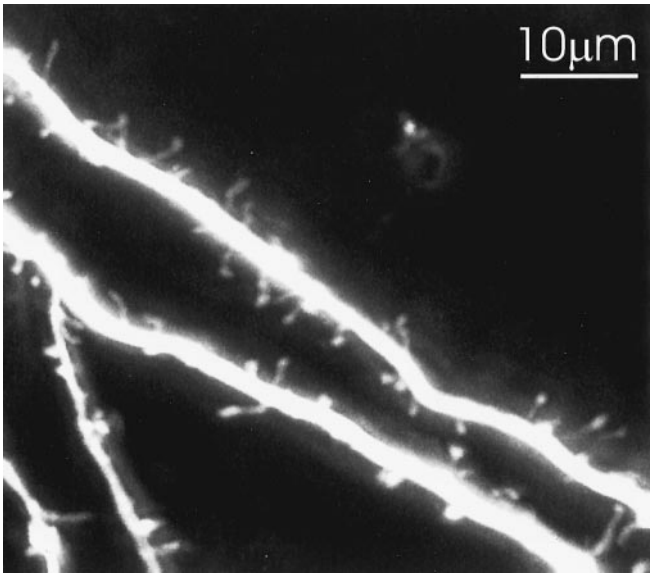

FIG. 3. High-resolution image of dendritic branches from CA1 pyramidal neurons expressing EGFP. Note numerous synaptic spines. The image is the maximum value projection of an image stack (30 images collected in 0.5-μm steps) that was acquired ~100 μm below the slice surface.

IMAGING GREEN FLUORESCENT PROTEIN

Expression of the recombinant green fluorescent protein (GFP) alone and as part of fusion proteins affords a number of exciting possibilities in cellular neuroscience. Today, wild-type GFP is rarely used. A mutant with improved fluorescence, "enhanced GFP" (EGFP), offers superior performance (18). Other mutants with other useful absorption and emission wavelengths also have been developed (19, 20). In addition, a number of functional GFPs have recently been described, designed to report either [Ca^{2+}] levels (21), membrane potentials (22), or pH (23). We have used EGFP as a cytoplasmic dye and as a part of fusion proteins to monitor their cellular distribution over time.

Cultured Slice Preparation

Hippocampal slice cultures were made from 6- to 8-day-old Sprague–Dawley rat pups as described (24). The brain was dissected out in ice-cold Hepes-buffered Hanks' solution (pH 7.35). Dissection of the hippocampus was carried out in a laminar-flow hood under ster-

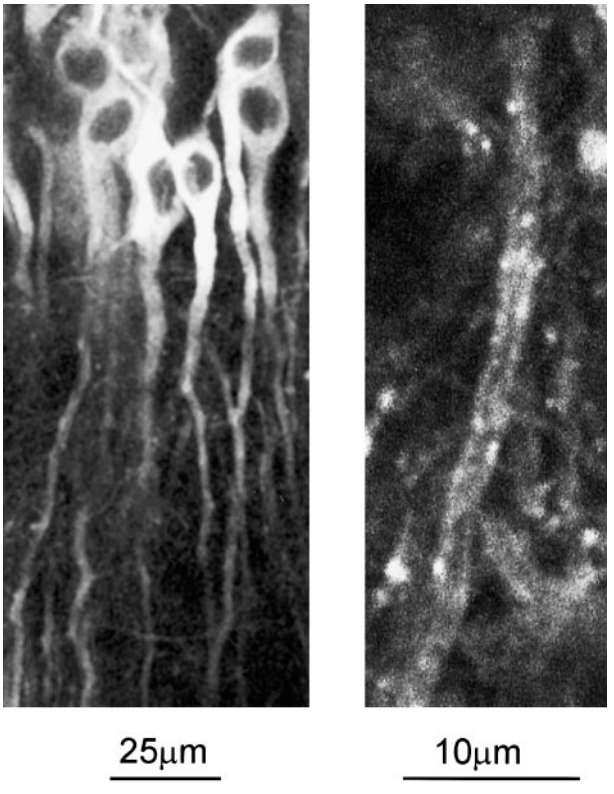

FIG. 4. CA1 pyramidal cells expressing GluR1–EGFP imaged in a cultured hippocampal brain slice. (Left) A cluster of neurons showing nuclear exclusion of the GluR1–EGFP construct. The image is a projection of four sections collected 0.5 μm apart. (Right) High-magnification image showing distribution of GluR1–EGFP in a dendritic branch. The image is a projection of 10 sections collected 0.5 μm apart.

ile conditions under a dissecting microscope. Hippocampi were sectioned on a tissue chopper and explanted onto a membrane (Millicell-CM, 0.4-μm pore size; Millipore). The membranes were then placed in 0.750 ml of culture medium for organotypic slices [MEM (Gibco 41200-072), 30 mM Hepes, 20% heat-inactivated horse serum, 1.4 mM glutamine, 16.25 mM D-glucose, 5 mM $NaHCO_3$, 1 mM $CaCl_2$, 2 mM $MgSO_4$, 1 μg/ml insulin, 0.012% ascorbic acid, pH 7.28, osmolarity 320]. Cultured slices were maintained at 35°C, in a humidified incubator (ambient air enriched with 5% CO_2). Culture medium was replaced every second day. Slices were cultured on the interface membrane for up to 3 weeks.

Viral Gene Delivery

The EGFP and EGFP fusion constructs were introduced into neurons using a Sindbis viral vector expression system (25). Cultured hippocampal slices were infected with the virus after 2–10 days *in vitro* by pressure injection (26). Expression of the recombinant EGFP was allowed for 1–4 days. A piece of membrane with an infected slice was cut out and transferred to a perfusion chamber under the TPLSM microscope. Slices were continuously perfused with preheated (28–32°C), oxygenated artificial cerebrospinal fluid (ACSF) containing 119 mM NaCl, 2.5 mM KCl, 4 mM $MgCl_2$, 4 mM $CaCl_2$, 1 mM NaH_2PO_4, 26.2 mM $NaHCO_3$, 11 mM glucose, and 100 μM picrotoxin. A cut was made between CA3 and CA1 regions to prevent epileptiform activity. Depending on the titer of the virus, from a few to most neurons in a slice can be infected in this manner.

GFP as a Cytoplasmic Dye

EGFP by itself is a soluble protein and appears to be homogeneously distributed within the cytosol of hippocampal neurons when expressed (Fig. 3). EGFP has major advantages compared with synthetic cytoplasmic dyes. Under our conditions, EGFP fluorescence is extremely bright, unveiling detailed structure including tiny dendritic spines, axonal boutons, and filopodia (Fig. 3) EGFP also appears to be very photostable compared with xanthene-based dyes (27), and produces very low levels of phototoxicity. In addition, dye delivery using genetic techniques leaves neurons relatively unperturbed, at least compared with the insult produced by microelectrode penetration required for delivery of synthetic dyes. Thus EGFP is an ideal tool for long-term imaging of morphological dynamics at high resolution in living tissue.

GFP Fusion Proteins

The distribution of EGFP fusion proteins can reveal the distribution of endogenous proteins. Care should be taken to avoid placing the EGFP tag near regions of the protein expected to confer targeting functions. For instance, we have placed EGFP at the amino terminus of

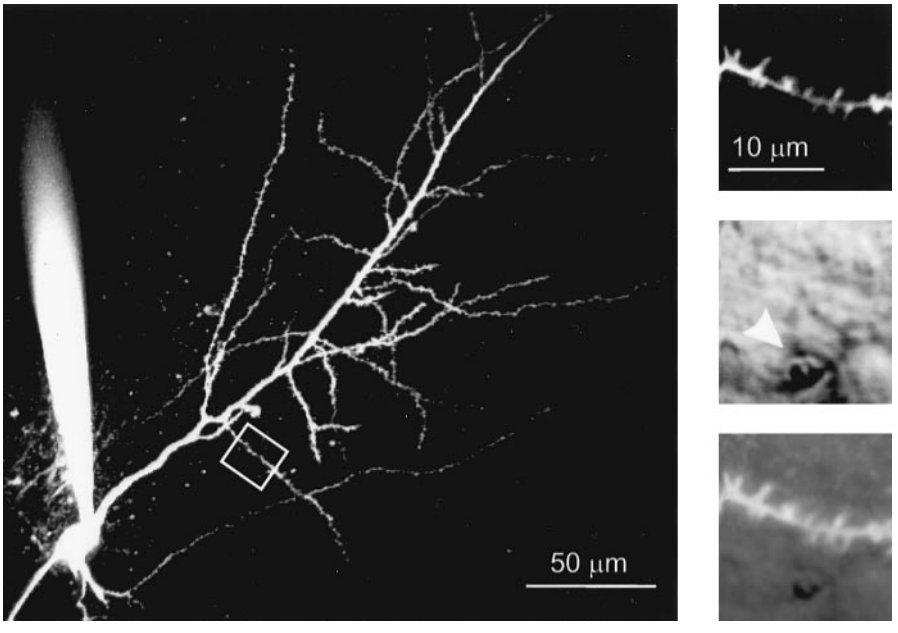

FIG. 5. CA1 pyramidal cell filled with OGB 1 (200 μM) via a patch pipet. The whole-cell image at left is the maximum value projection of a stack of images (50 sections at 0.5-μm spacing, 512 × 512 pixels/section). The right panels show a thin spiny dendrite from the same cell (stack of 20 images at 0.5-μm steps; the location and size are indicated by the white box in the left panel) at the higher magnification used for locating active synapses. Also shown is the corresponding LSDIC image of the stimulating electrode (arrow, middle) and superposition of fluorescence stack and LSDIC images (bottom).

the AMPA receptor subunit GluR1 (Fig. 4). This region of the protein is predicted to be extracellular (28). In contrast, the targeting regions of GluR proteins have been mapped to the C terminus. In our experience, EGFP fusion proteins are expressed at relatively low levels compared with plain EGFP; low signal levels can therefore be a problem. This is especially true with membrane proteins. For example, if every glutamate receptor in a synapse was tagged by an EGFP molecule each synapse would light up with only about 10–100 fluorophores. In the case of free EGFP, the cytoplasm of a dendritic spine can be filled up with thousands of fluorophores. The imaging of subcellular distributions of EGFP-tagged proteins therefore requires careful attention to detail with respect to signal detection, especially in the slice. In the images of Fig. 4, an inhomogeneous distribution of the fusion protein (GluR1–EGFP) can clearly be made out.

FUNCTIONAL SYNAPTIC IMAGING USING [Ca^{2+}] INDICATORS

TPLSM allows the imaging of [Ca^{2+}] dynamics in individual spines in brain slices. This is of profound interest for at least two reasons: First, synaptic activation can produce postsynaptic Ca^{2+} influx, and the resulting Ca^{2+} accumulation is thought to trigger the biochemical cascades underlying the induction of long-term potentiation (LTP) and other forms of plasticity (29). Second, synaptically evoked spine [Ca^{2+}] reports the release of a presynaptic vesicles and can therefore be used to measure the stochastic properties of individual synapses (30).

Acute Slice Preparation

Hippocampal slices were prepared from juvenile rats or mice (14–28 days postnatal). The brain was removed, sections of brain containing the hippocampus were blocked, and 300- to 400-μm-thick slices were cut on a Vibratome. These procedures were all carried out with the brain submerged in a choline chloride-based, chilled (2–5°C) ACSF bubbled with carbogen (95% O_2/5% CO_2). The cutting solution, which was designed to maximize slice health (31), was composed of (in mM) 110 choline chloride, 25 $NaHCO_3$, 25 D-glucose, 11.6 sodium ascorbate, 7 $MgSO_4$, 3.1 sodium pyruvate, 2.5 KCl_2, 1.25 NaH_2PO_4, and 0.5 $CaCl_2$. Slices were then transferred to a submerged holding chamber containing normal ACSF and incubated at 35°C for ~1 h and then held at room temperature until used. The composition of the normal ACSF was (in mM) 127 NaCl, 25 $NaHCO_3$, 25 D-glucose, 2.5 KCl, 2 $CaCl_2$, 1 $MgCl_2$, 1.25 NaH_2PO_4. The $MgCl_2$ was increased to 2 mM in the holding chamber and decreased to 0.1 mM in some experiments. Picrotoxin (0.1 mM) was routinely added to block $GABA_A$ receptors; a cut was made between the CA3 and CA1 regions to prevent epileptiform activity.

Perfusion and Temperature Control

For electrical and optical recording, slices were placed in a submerged chamber (0.5 ml) and perfused with temperature-controlled ACSF using a recirculating system (50-ml total solution volume). In a 50-ml

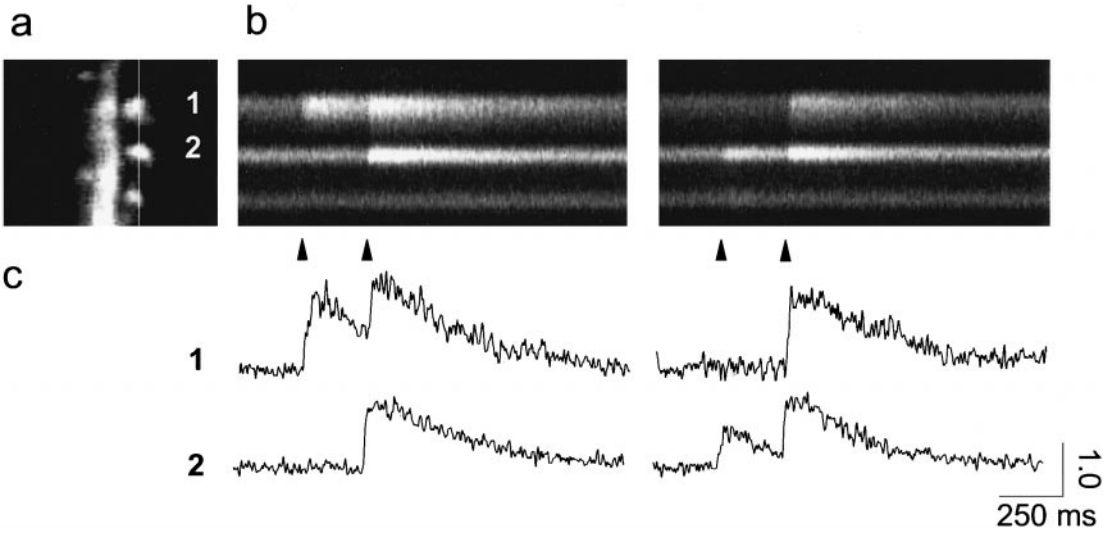

FIG. 6. Fast line-scan measurements of synaptic [Ca^{2+}] transients in individual spines. (a) Fluorescence image of a tertiary dendrite with three spines. The line indicates the location of the line scan. The active spines are numbered (1, 2). (b) Raw line-scan images showing two trials in which pairs of synaptic stimuli were delivered at 256-ms intervals. The line-scan images have one space dimension (vertical) and one time dimension (horizontal). (c) The data shown in (b) are averaged over a small window in the vertical dimension and plotted as $\Delta F/F$ time series for the numbered spines.

reservoir, the ACSF was bubbled with carbogen and preheated to prevent later degassing. The solution was gravity fed (2–3 ml/min) to the recording chamber and returned to the reservoir by a peristaltic pump. Final temperature control (e.g., 35 ± 1°C) was maintained using an in-line heater (Warner Instruments) equipped with a feedback thermistor placed in the recording chamber.

Whole-Cell Recording

Whole-cell recordings were used to introduce the [Ca^{2+}] indicator into the cell, monitor synaptic transmission, and control the postsynaptic holding potential. Recordings were obtained under visual guidance using IRDIC optics with a CCD camera (Hamamatsu). LSDIC was not used to guide recordings due to limitations of the image acquisition rate. The patch electrodes (2–4 MΩ) were filled with a solution containing (in mM) 135 cessium methylsulfonate or potassium methylsulfate, 10 Hepes, 10 sodium phosphocreatine, 4 $MgCl_2$, 4 Na_2-ATP, 0.4 Na-GTP, as well as 0.1 to 1 mM of a chosen [Ca^{2+}] indicator. Voltage-clamp recordings and the Cs^+-based internal solution were used to prevent spiking of the postsynaptic cell and to control the holding potential of the cell. Current-clamp recordings and the K^+-based internal solution allowed more physiologically neutral recordings. A K^+-based solution was also used to patch the cell temporarily, allowing intracellular delivery of the Ca^{2+} indicator. With such a protocol it was possible to continue imaging without simultaneous electrical recording for periods of several hours.

Synaptic Stimulation

To maximize the chances of locating active synapses, transmission was evoked using an extracellular electrode placed within a few micrometers of a target dendrite. We used a glass pipet filled with ACSF (tip diameter 2–4 μm), through which 1- to 10-V, 0.1-ms constant-voltage pulses were delivered. To facilitate placement of the electrode, a bend was made using a microforge (Narashige) so that the last ~200 μm of the shaft was perpendicular to the surface of the slice. Using a motorized micromanipulator (Sutter) with orthogonal *Z* axis allowed the electrode tip to be easily positioned to within 5–10 μm of a desired location and minimized disurbance of the tissue when lowering the electrode into the slice. Before recording, the tip of the stimulating pipet was positioned above the soma of the target cell. After gaining whole-cell access under IRDIC, we switched to TPLSM (Fig. 5). As the cell filled with Ca^{2+} indicator, baseline measurements of action potential-evoked [Ca^{2+}] transients were taken to estimate free Ca^{2+} and indicator levels. After 5–15 min for filling, a target secondary or tertiary dendritic branch (50–200 μm from the cell body) was located by moving the scanning field (~10 × 10 μm) away from the soma following the dendrite. Movement of the field was achieved by moving the microscope stage. The coordinates of the region of interest were determined by digital micrometers (*X*,*Y* axis) and a computer-controlled focus motor driver (*Z* axis). Using the soma as a reference location, the stimulation pipet was maneuvered to the target dendritic location (*X*,*Y*) and then lowered (*Z*) to the target branch (see Fig. 5). Active spines were identified by imaging at intermediate temporal and spatial resolution (128 pixels square, 6 frames at 256 ms/frame) as the stimulus intensity was gradually increased. This procedure gave high "hit rates" (i.e., locating active spines within the target dendritic region). Based on the size and fluctuations of synaptic currents evoked, we estimate that synaptic activation also occurred outside of the field of view.

Measurement of Synaptic Function

Limitations in the number of photons emitted from small structures such as dendritic spines and in the acquisition and/or scanning rates of most imaging systems necessitate a compromise between spatial and temporal resolution when measuring synaptic [Ca^{2+}] signals. When temporal resolutions on the order of ~10 Hz are acceptable, it is preferable to monitor transmission at multiple individual synaptic sites by acquiring movies. This allows measurements of [Ca^{2+}] over a whole dendritic branch and brings the additional benefit of a substantial reduction in peak laser dosage. With this method, synaptic transmission can be monitored over the course of hundreds of stimulation trials without damaging the imaged structures (Fig. 1a). The main limiting factor on the number of measurements that can be collected from a single field is the maintenance of a low background Ca^{2+} level. Even relatively small increases in resting [Ca^{2+}], which typically accompany deteriorating cellular health, can significantly compromise the dynamic range of high affinity Ca^{2+} indicators. When electrical measurements or voltage control is not necessary, long-term viability can be improved by terminating the whole-cell recording by careful withdrawal of the pipet. When high temporal resolution is necessary, the preferred acquisition method is the so-called "line-scan" mode in which scanning in the slow axis is turned off (Fig. 6). Temporal resolutions in the millisecond range can be achieved.

CONCLUSIONS

TPLSM is rapidly becoming a mature tool in cellular neuroscience. Simple TPLSM microscopes allow high-resolution fluorescence imaging with minimal photodamage deep in scattering tissue. We expect that fu-

ture technical advances will continue to increase the range of applicability for this exciting technique.

ACKNOWLEDGMENTS

We thank Barry Burbach and Peter O'Brien for technical assistance, Winfried Denk for various insights and discussions, and Winfield Hill for help with electronics. The scanning software used was written at Bell Laboratories, Lucent Technologies. Parts of this work were funded by a Burroughs Wellcome Career Development Award (Z.F.M.); NINDS and Mathers Charitable Foundation (R.M.); the Pew and Whitaker Foundations and a Human Frontiers Research Grant (K.S.).

REFERENCES

1. Denk, W., and Svoboda, K. (1997) *Neuron* **18,** 351–357.
2. Dodt, H. U., and Zieglgansberger, W. (1994) *Trends Neurosci.* **17,** 453–458.
3. Stuart, G. J., Dodt, H. U., and Sakmann, B. (1993) *Pfluegers Arch.* **423,** 511–518.
4. Denk, W., Strickler, J. H., and Webb, W. W. (1990) *Science* **248,** 73–76.
5. Denk, W., Yuste, R., Svoboda, K., and Tank, D. W. (1996) *Curr. Opin. Neurobiol.* **6,** 372–378.
6. Svoboda, K., Tank, D. W., and Denk, W. (1996) *Science* **272,** 716–719.
7. Yuste, R., and Denk, W. (1995) *Nature* **375,** 682–684.
8. Denk, W., Sugimori, M., and Llinas, R. (1995) *Proc. Natl. Acad. Sci. USA* **92,** 8279–8282.
9. Denk, W., Piston, D. W., and Webb, W. W. (1995) *in* Handbook of Biological Confocal Microscopy (Pawley, J. B., Ed.), pp. 445–458, Plenum, New York.
10. Svoboda, K., Denk, W., and Tank, D. W. (1998) *in* Imaging Living Cells (Yuste, R., Lanni, F., and Konnerth, A., Eds.), Cold Spring Harbor Press, Cold Spring Harbor, NY.
11. Svoboda, K., Denk, W., Kleinfeld, D., and Tank, D. (1997) *Nature* **385,** 161–165.
12. Gosnell, T. R., and Taylor, A. J. (1991) *in* Milestone Series, SPIE Press, Bellingham, WA.
13. Xu, C., Zipfel, W., Shear, J. B., Williams, R. M., and Webb, W. W. (1996) *Proc. Natl. Acad. Sci. USA* **93,** 10763–10768.
14. Muller, M., Squier, J., and Brakenhoff, G. J. (1995) *Opt. Lett.* **20,** 1038–1040.
15. Guild, J. B., Xu, C., and Webb, W. W. (1997) *Appl. Opt.* **36,** 397–401.
16. Pawley, J. B. (1995) Handbook of Biological Confocal Microscopy, Plenum, New York.
17. Horowitz, P., and Hill, W. (1989) The Art of Electronics, pp. 1–1125, Cambridge Univ. Press, Cambridge.
18. Cormack, B. P., Valdivia, R. H., and Falkow, S. (1996) *Gene* **173,** 33–38.
19. Cubbit, A. B., *et al.* (1995) *Trends Biochem. Sci.* **20,** 448–455.
20. Heim, R., and Tsien, R. Y. (1996) *Curr. Biol.* **6,** 178–182.
21. Miyawaki, A., *et al.* (1997) *Nature* **388,** 882–887.
22. Siegel, M. S., and Isacoff, E. Y. (1997) *Neuron* **19,** 735–741.
23. Kneen, M., Farinas, J., Li, Y., and Verkman, A. S. (1998) *Biophys. J.* **74,** 1591–1599.
24. Stoppini, L., Buchs, P. A., and Muller, D. A. (1991) *J. Neurosci. Methods* **37,** 173–182.
25. Schlesinger, S. (1993) *Trends Biotechnol.* **11,** 18–22.
26. Malinow, R., *et al.* (1998) *in* Imaging Living Cells (Yuste, R., Lanni, F., and Konnerth, A., Eds.).
27. Pierce, D. W., Hom-Booher, N., and Vale, R. D. (1997) *Nature* **388,** 338.
28. Hollman, M., Maron, C., and Heinemann, S. (1994) *Neuron* **13,** 1331–1343.
29. Bliss, T. V. P., and Collinridge, G. L. (1993) *Nature* **361,** 31–39.
30. Stevens, C. F. (1993) *Cell* **72,** 55–63.
31. Lipton, P., *et al.* (1995) *J. Neurosci. Methods* **59,** 151–156.